第38卷第1期 无 机 化 学 学 报 Vol.38 No.1
2022年1月 CHINESE JOURNAL OF INORGANIC CHEMISTRY 153-160

Mn-MOF衍生的Mn_2O_3微马达用于水中甲基蓝的去除

黄 婧 田欣雨 杨 澜 冯晓苗*
(南京邮电大学材料科学与工程学院,省部共建有机电子与信息显示国家重点实验室,
信息材料与纳米技术研究院,南京 210023)

摘要: 以锰金属有机框架(Mn-MOF)为前驱体制备了Mn_2O_3微球。所得微球大小约为4 μm,尺寸均匀,具有完美的球形结构,表面粗糙,结晶度好,产率较高。同时,研究了Mn-MOF衍生的Mn_2O_3微马达在不同条件下的运动性能以及对甲基蓝的降解性能。Mn_2O_3微马达运动性能优异,在10%的H_2O_2溶液中,其运动速度可达81.32 μm·s^{-1}。实验结果表明,加入H_2O_2后,Mn_2O_3微马达在5 min内通过降解作用可有效去除MB。

关键词: 自驱动; 微马达; Mn_2O_3; 降解; 甲基蓝
中图分类号: TB34; O614.71+1 **文献标识码:** A **文章编号:** 1001-4861(2022)01-0153-08
DOI: 10.11862/CJIC.2022.008

Mn-MOF Derived Mn_2O_3 Micromotors Applied to Removal of Methyl Blue in Water

HUANG Jing TIAN Xin-Yu YANG Lan FENG Xiao-Miao*
(*Key Laboratory for Organic Electronics and Information Displays & Institute of Advanced Materials* (*IAM*),
School of Materials Science & Engineering, Nanjing University of Posts & Telecommunications, Nanjing 210023, *China*)

Abstract: A Mn-based metal-organic framework (Mn-MOF) was selected as the precursors to prepare the Mn-MOF derivative (Mn_2O_3) microspheres. The Mn_2O_3 microspheres had a homogenous size of *ca*. 4 μm, with perfect sphere morphology, rough surface, good crystallinity and high yield. At the same time, the movement behavior of Mn_2O_3 micromotors under different conditions and the degradation properties of methyl blue (MB) were studied. As-prepared Mn_2O_3 micromotors had excellent autonomous movement ability, and their moving speed can reach 81.32 μm·s^{-1} in 10% H_2O_2 solution. Experimental results show that with the addition of H_2O_2, the Mn_2O_3 micromotors can effectively remove MB through degradation within 5 min.

Keywords: self-propelled; micromotor; Mn_2O_3; degradation; methyl blue

0 Introduction

Micro/nanomotors are a class of micro/nanoscale devices which can convert external energy or chemical substances into driving forces to realize autonomous movement. According to the propulsion mechanism[1], they can be categorized into physical-driven (including light energy[2], magnetic field[3], ultrasonic wave[4], electric field[5], and thermal energy[6]) and fuel-driven (*e.g.*, H_2O_2[7], glucose[8], lactose[9], and urea[10]). Fuel-driven micro/nanomotors are powered by catalytic reactions which present high speed and efficiency. A large number of catalytic materials have been used in the design of fuel-driven micro/nanomotors. Traditional catalysts including noble metals (*e.g.*, Pt[11], Ag[12]), active metals (*e.g.*, Mg[13], Zn[14]), metal oxides (*e.g.*, MnO_2[15], Fe_2O_3[16]),

收稿日期:2021-07-09。收修改稿日期:2021-09-28。
国家自然科学基金(No.62174087)资助。
*通信联系人。E-mail:iamxmfeng@njupt.edu.cn

or enzymes[17], have excellent catalytic performances. However, some of these materials have problems of high cost and complicated preparation process, which are not conducive to large-scale production and practical application. Therefore, the development of low-cost, easy-to-prepare and high catalytic activity micro/nanomotor materials still faces major scientific challenges.

The extensive application of micromotors has been made great progress in explosives detection[18], biomedicine[19], environmental restoration[20], nano engineering[21] and other fields for the past few years. At present, the issue of environmental restoration, especially sewage treatment, is a huge challenge facing the world[22]. Generally, organic pollutants in water are removed by physical adsorption and chemical oxidation. Micro/nanomotors have a promising potential application in this field and many works have been reported to date. Liang et al. used silver nano-colloids as the surface-enhanced Raman scattering (SERS) substrate to introduce SERS technology, and designed micro/nanomotors with water quality monitoring functions, which could identify the characteristic peaks of pollutants in the SERS spectrum of the resulting solution[23]. The combination of micro/nanomotors and sensing technology provided a new direction for environmental monitoring. Ma et al. prepared Janus micromotor by incorporating iron ions into the zeolite framework[24]. The micromotors used Pt to catalyze H_2O_2 to generate driving force, while iron ions catalyze H_2O_2 to continuously generate hydroxyl radicals, which degraded phenol as a model pollutant. Similarly, Shi et al. used reduced graphene oxide (rGO) to immobilize Fe_3O_4 nanoparticles (NPs) to synthesize heterogeneous Fe_3O_4-rGO/Pt microjets which could improve the degradation capability of Fenton composite microjets and effectively remove methylene blue in a short time[25]. In response to recent oil spills, many researchers had applied micro/nanomotors to dynamic oil removal. The canned hollow $MnFe_2O_4$ micromotor could quickly and efficiently collect oil droplets through the hydrophobic surface-oil interaction of the pre-existing long oleic acid chains[26]. For the first time, Luis et al. used the wax printing template-assisted rolled-up method to prepare rGO/Pt tubular micromotors[27]. The hydrophobicity and high specific surface area to volume ratio of rGO provided favorable conditions for reversibly collecting and releasing oil in water. The removal and recycling of heavy metal from sewage are also crucial in environmental remediation issues. A multi-functional mesoporous silica-based microinjector was immobilized MnO_2 and γ-Fe_2O_3 NPs on the inner and outer surface, respectively[28]. The interaction between Fe_2O_3 NPs and heavy metals could remove heavy metal ions such as Cd^{2+} and Pb^{2+} in wastewater. And the microjets could be easily guided and recycled by a magnetic field. Hou et al. designed a self-propelled tubular micromotor based on a copolymer of aspartic acid and cysteine (PAsp-Cys), which could quickly remove inorganic and organic heavy metals in polluted water[29]. This was due to the strong binding force between sulfhydryl groups of PAsp-Cys and metals (especially mercury). Meanwhile, the multi-carboxyl and amino groups of PAsp were also used to adsorb various metal ions.

Metal-organic framework (MOF) with large pore size, stable crystal lattice, and functional groups is a kind of porous material assembled by metal ions and bridged organic ligands, which has attracted a lot of attention in recent years[30]. Therefore, the introduction of MOF materials into fuel-catalyzed micro/nanomotors, which increases the catalytically active sites and active surfaces of the micro/nanomotors, is expected to realize the efficient role of the micro/nanomotors in environmental remediation. Ikezoe et al. proposed the application of MOF materials to micromotors for the first time, which expanded the new research direction of micromotor preparation materials[31]. Recently, we have synthesized a spherical and dodecahedron-based ZIF-67 catalytic micromotor by changing the solvent in one step[32]. Owing to the higher surface area and hollow structure of ZIF-67, the micromotors can dramatically adsorb the methyl blue (MB) within 5 min.

A series of derivatives can also be obtained by using MOF as a precursor, which not only retains the original porosity and morphology of the precursor, but also exhibits stronger catalytic activity[33]. In this work, Mn_2O_3 micromotors were prepared by using Mn-MOF

as a precursor through high-temperature annealing. The size of Mn_2O_3 was about 4 μm, with a microporous structure and good crystallinity. At the same time, the movement behavior of Mn-MOF derivative micromotors under different conditions and the degradation properties of MB were studied. The prepared Mn_2O_3 micromotors had excellent autonomous movement ability, and their moving speed can reach 81.32 $\mu m \cdot s^{-1}$ in 10% H_2O_2 solution. The experimental results illustrate that after adding H_2O_2, the Mn_2O_3 micromotors showed a strong degradation effect on MB. These Mn_2O_3 micromotors using Mn-MOF as the precursor had lower material costs and are suitable for mass production. Compared with other external stimuli, such as light, ultrasound, magnetic field and temperature, H_2O_2 and the Mn_2O_3 micromotors had a Fenton-like reaction to efficiently degrade pollutants, and H_2O_2 can drive the micromotors to achieve autonomous movement simultaneously.

1 Experimental

1.1 Materials

Manganese acetate tetrahydrate ($Mn(CH_3COO)_2 \cdot 4H_2O$), MB and ethanol were purchased from Sinopharm Chemical Reagent Co., Ltd. Polyvinylpyrrolidone (PVP), 1,3,5-trimellitic acid, and 2-methylimidazole are commercially available from Aladdin Inc. Hydrogen peroxide (H_2O_2, 30%) was purchased from Shanghai Chemical Reagent Co., Ltd. Triton X-100 was purchased from Alfa Aesar Chemical Co., Ltd. The ultrapure water used in the experiment was purified by the Milli-Q system. All the reagents were analytical grade and used as received without further treatment.

1.2 Synthesis of Mn-MOF derivatives

Mn-MOF was prepared according to the reported method[34]. First, 0.49 g of $Mn(CH_3COO)_2 \cdot 4H_2O$ was dissolved in 100 mL of the mixture of water and ethanol (1∶2, *V*/*V*). After it was completely dissolved, 2 g of PVP was added under vigorously stirring until completely dissolved. It was recorded as solution A. Then, 0.9 g of 1,3,5-trimellitic acid was dissolved in the mixture of 80 mL of water and ethanol (1∶2, *V*/*V*). It was designated as solution B. Solution B was dropwise added to solution A under vigorous stirring and it was kept with stirring for 20 min, and then, the reaction was allowed to stand at room temperature for 12 h. After the reaction was completed, the solution was divided into two layers including the supernatant and the underlying white precipitate. The solution was centrifuged and the precipitate was washed using ethanol three times. The final product was dried under vacuum at 60 ℃ for 6 h to obtain Mn-MOF. The white powder of Mn-MOF was evenly spread on the bottom of the porcelain boat. The outer layer of the porcelain boat was covered with tin foil. The porcelain boat was placed in a muffle furnace. The temperature was programmed at 700 ℃ at a heating rate of 10 $℃ \cdot min^{-1}$ and held for 3 h at 700 ℃. After the end of the procedure, it was naturally cooled to room temperature to get black Mn-MOF derivatives.

1.3 Characterization

The composition of Mn-MOF and Mn-MOF derivative micromotors was characterized by X-ray diffraction (XRD, BRUKER D8 Advance, Cu $K\alpha$, λ=0.154 001 nm, 2θ=10°-80°, 40 kV, 40 mA) and FT-IR (Bruker model VECTOR-22 Fourier transform spectrometer). Thermogravimetric analysis (TGA) was performed in air atmosphere using a differential scanning calorimeter (DSC214 polyma). The microscopic morphology was observed by a scanning electron microscope (SEM, Hitachi S-4800, 3 kV) and a transmission electron microscope (TEM, Hitachi HT7700, 100 kV). Chemical bond analysis was performed by X-ray photoelectron spectroscopy (XPS, PHI 5000 Versa Probe), and UV-Vis absorption spectroscopy was performed by a UV-Vis spectrometer (PerkinElmer, Lambda 650S). Motion videos were recorded by an inverted fluorescence microscope (Ti-S/L100). The calculation and analysis of motor speed were done by NIS-Elements software. Before the motion experiment, Mn-MOF derivatives were coated with a 10 nm-gold layer by the E-1010 ion sputter.

2 Results and discussion

The morphologies of Mn-MOF and its derivative were characterized by SEM and TEM, as shown in Fig. 1. From Fig. 1a and 1b, we can see that the Mn-

MOF precursor showed a perfectly sphere shape with a smooth surface and an average diameter was about 4 μm. After annealing in the muffle furnace from 400 to 700 ℃, it still maintained relatively complete spherical morphology without cracking (Fig.1c, 1d; Fig.S1a-S1c in Supporting information). However, the surface of the sphere became rough after annealing, which may be due to the release of gas molecules caused by the decomposition of Mn-MOF during annealing. As presented in Fig. S1d, when the annealing temperature reached 800 ℃, its spherical morphology was obviously broken. Video S1 (Supporting information) shows that the motion performance of derivatives of Mn-MOF obtained at annealing temperatures of 700 ℃ was better than those of the samples obtained at 400, 500, and 600 ℃. Therefore, we choose the Mn-MOF derivative obtained at an annealing temperature of 700 ℃ for subsequent research.

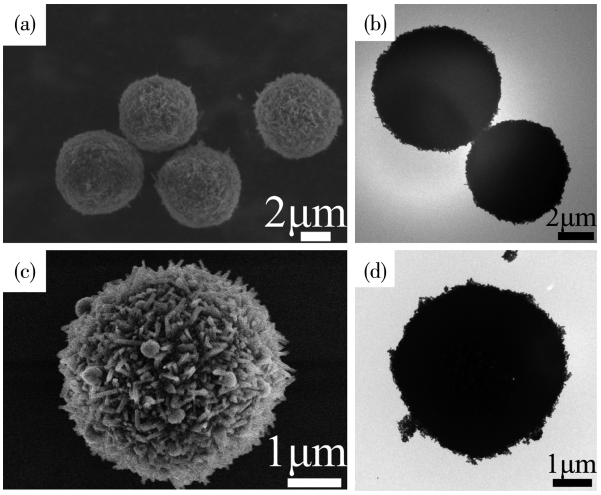

Fig.1 SEM (a, c) and TEM (b, d) images of Mn-MOF (a, b) and its derivative obtained at an annealing temperature of 700 ℃ (c, d)

The structures of Mn-MOF and its derivative were further analyzed by XRD, as shown in Fig. 2a. The Mn-MOF precursor exhibited similar characteristic peak with the reference[34]. After annealing, the diffraction peaks are consistent with Mn_2O_3 completely (PDF No.41-1442, lattice constant a=0.940 9 nm), indicating the perfect crystallinity and high purity of the product.

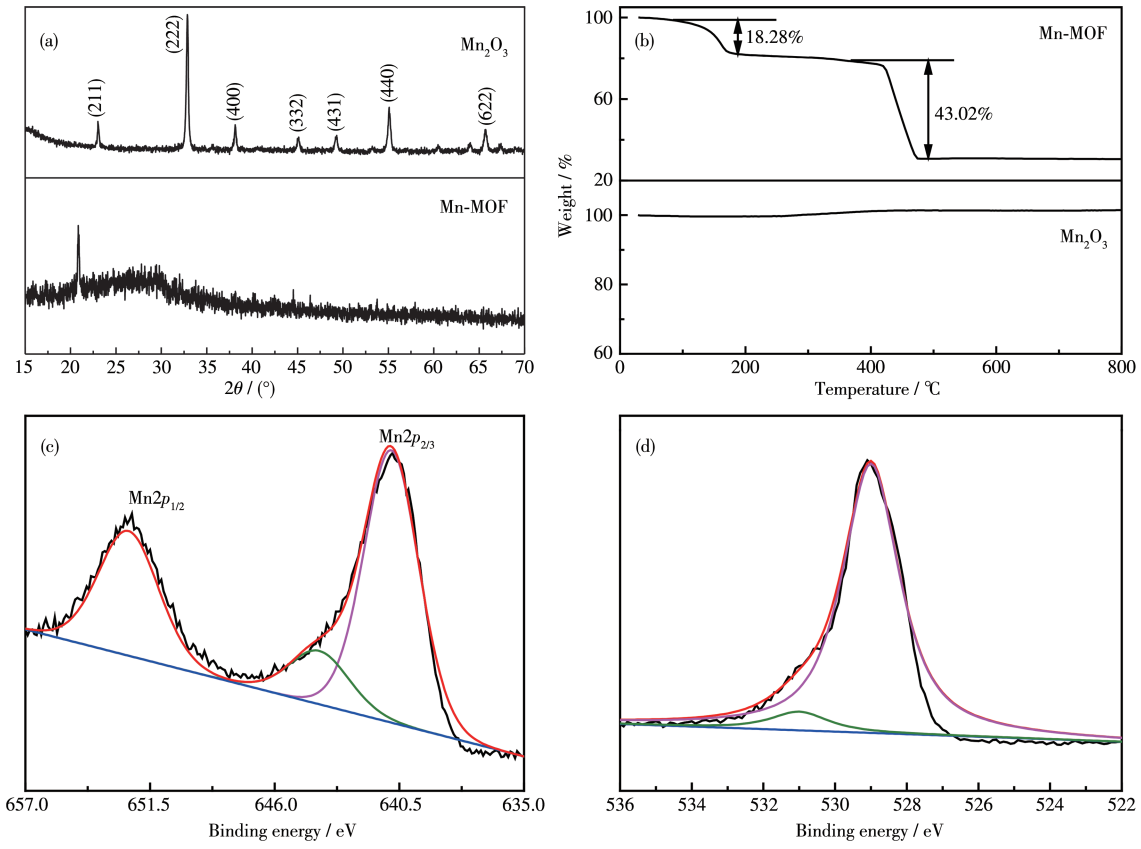

Fig.2 XRD patterns of Mn-MOF and its derivative (a); TGA curves of Mn-MOF and its derivative (b); XPS spectra of Mn2p (c) and O1s (d) of the derivative of Mn-MOF

As shown in the TG curve of Mn-MOF (Fig.2b, top), the first 18.28% weight loss around 200 ℃ is attributed to the loss of lattice water. The second weight loss around 480 ℃ originates from the thermal decomposition of the sample, indicating that Mn-MOF has a stable crystal structure above 480 ℃. The TGA curve (Fig.2b, bottom) of Mn_2O_3 derived from Mn - MOF showed no change within the temperature range illustrating it has good thermal stability. The XPS results show that there are two elements (Mn and O) in the sample. Fig. 2c shows the high-resolution XPS spectrum of Mn2*p*. The peaks of Mn2$p_{1/2}$ and Mn2$p_{3/2}$ were situated at 652.4 and 641.2 eV, respectively. The peaks appearing at 640.8 and 643.9 eV correspond to Mn^{3+} and Mn^{4+}, respectively[35]. As shown in Fig.2d, the peaks of O1*s* at 529.0 and 531.0 eV correspond to crystal lattice oxygen and the surface adsorbed oxygen species in Mn_2O_3, respectively. The result is well consistent with that of the XRD analysis.

The Mn_2O_3 micromotors derived from Mn - MOF can move efficiently by decomposing H_2O_2. Fig.3a and 3b display time-lapse images taken from Video S1 in a 2 s period powered by different H_2O_2 concentrations. These images illustrate a tail of oxygen bubbles generated and released from the Mn_2O_3 surface. Video S1 shows that the Mn_2O_3 micromotors display autonomous locomotion with different speeds in different H_2O_2 concentrations. The concentration of H_2O_2 fuel strongly influences the velocity of the Mn_2O_3 micromotors. Fig. 3c shows the relationship between micromotors′ speed and H_2O_2 concentrations. When the H_2O_2 concentration was increased from 1% to 10%, the speed of the micromotors was correspondingly increased from 21.71 to 81.32 μm·s^{-1} with an average lifetime of about 30 min.

In this work, MB was selected as a model pollutant to study the removal performance of Mn_2O_3 micromotors. To analyze the removal process of MB, the absorption peaks of MB in solution were measured by the UV - Vis spectrometer. The maximum absorption wavelength of MB was 598 nm. Fig.4 shows the changes of UV absorbance of different samples with time. As shown in curves a and b, the absorbance of MB did not change without or with H_2O_2, indicating that H_2O_2 has no effect on the removal of MB. It can be seen that the absorbance of MB decreased only after adding Mn_2O_3 micromotors (curve c), which further proves that Mn_2O_3 has an adsorption effect on MB. As shown in curve d, after adding Mn_2O_3 micromotors and H_2O_2 to MB solution simultaneously, the absorbance of MB was significantly reduced, which indicates that the Fenton-like system composed of Mn_2O_3 micromotors and H_2O_2 exhibits higher degradation efficiency for MB than the adsorption performance of pure Mn_2O_3.

FT-IR measurements were performed to study the removal mechanism of MB. Fig. 5 shows the FT - IR spectra of Mn_2O_3 (a), MB (b), mixed Mn_2O_3 and MB solution without H_2O_2 (c) or with H_2O_2 (d). In curve a, the characteristic absorption peaks at 612 and 529 cm^{-1} correspond to the asymmetric and symmetric Mn—O—Mn stretching vibrations in Mn_2O_3, respectively[36]. Curve b shows that the characteristic absorption peaks at 1 575 and 1 496 cm^{-1} correspond to the stretching vibrations of the C═C and C═N groups in

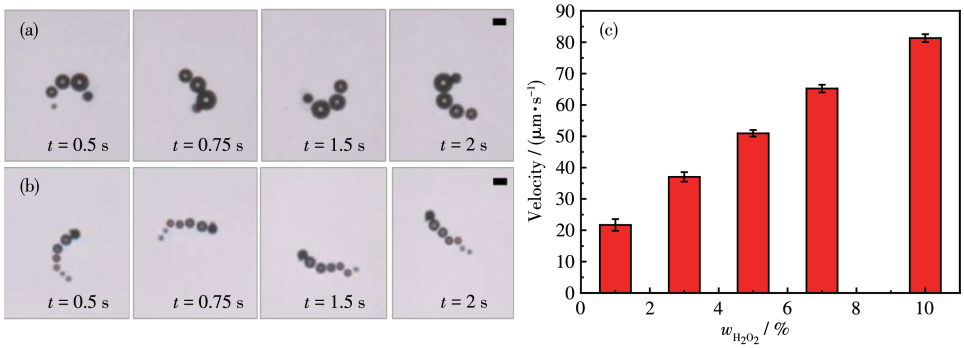

Fig.3　Time-lapse images of Mn_2O_3 micromotors in different concentrations (a: 1%, b: 7%) of H_2O_2; Relationship between micromotors′ speed and H_2O_2 concentration (c)

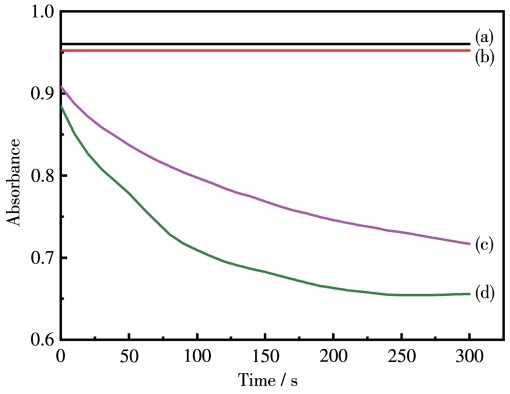

Fig.4 Changes of absorbances of different samples with time: (a) MB, (b) MB and H_2O_2 solution, (c) MB and Mn_2O_3 micromotors, (d) MB, Mn_2O_3 micromotors and H_2O_2 solution

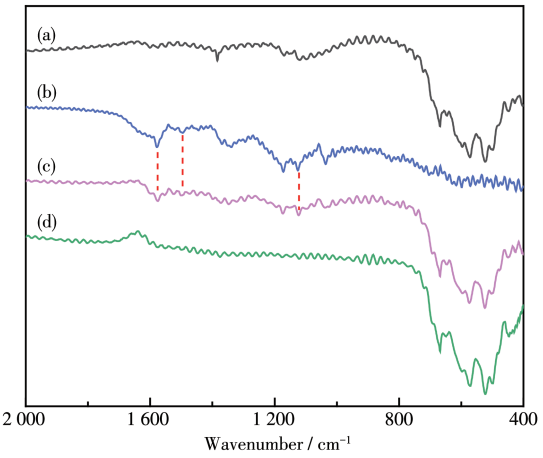

Vertical dotted line indicates the bond stretching mode of MB

Fig.5 FT-IR spectra of Mn_2O_3 (a), MB (b), mixed Mn_2O_3 and MB solution without H_2O_2 (c) or with H_2O_2 (d)

MB, respectively. The peak located at 1 169 cm^{-1} corresponds to the stretching vibration of the S=O group. Compared with pure Mn_2O_3 (curve a), the characteristic absorption peak of MB appears additionally in curve c, which indicates that in the absence of H_2O_2, Mn_2O_3 exhibits an adsorption effect on MB. However, the absorption peak of MB was not observed in curve d, which proves that in the presence of H_2O_2, Mn_2O_3 micromotors exhibit degradation effect rather than adsorption to MB.

Based on the above discussions, the likely catalytic mechanism for the activation of H_2O_2 by Mn_2O_3 micromotors in the degradation of organic pollutants through the Fenton-like effect is proposed as follows. Firstly, Mn^{3+} on the surface of Mn_2O_3 is easily reduced by H_2O_2 to produce Mn^{2+}, H^+ and $HO_2\cdot$ under near-neutral conditions. Then, Mn^{2+} reacts with H_2O_2 to produce Mn^{3+}, HO^- and $\cdot OH$. Therefore, Mn_2O_3 can decompose H_2O_2 cyclically and produce a large number of reactive oxygen species ($HO_2\cdot$, $\cdot OH$), which realizes the effect of the micromotor to remove MB[37]. Moreover, after adding Mn_2O_3 micromotors and H_2O_2 to the MB solution simultaneously, Mn_2O_3 contacts with H_2O_2 in the solution to continuously generate bubbles, which not only promotes the movement of the micromotors to achieve mixing, but also accelerates the degradation process without the need of external mechanical stirring.

Fig.6 presents that the amount of Mn_2O_3 micromotors and time has a direct effect on the degradation of MB. It shows that different amounts of Mn_2O_3 micromotors degraded the MB sample with the same concentration within 5 min. With the increase of the amount of

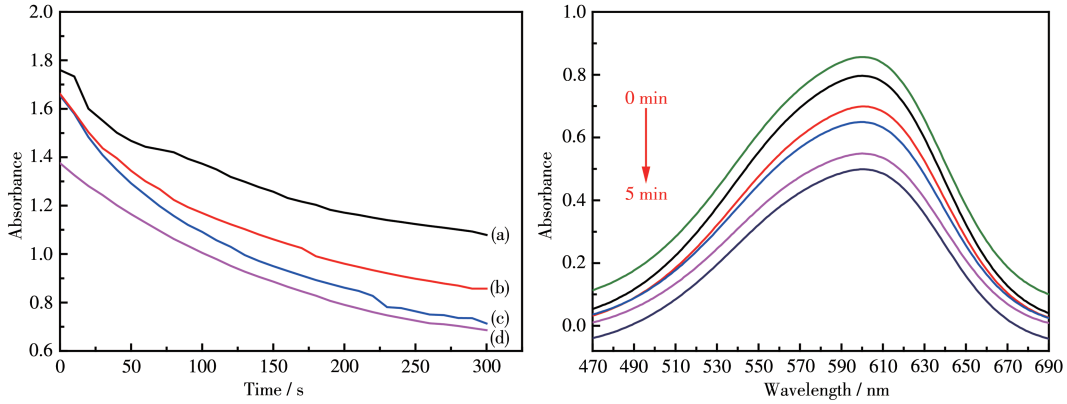

(a) 1 mg·mL^{-1}, (b) 2 mg·mL^{-1}, (c) 3 mg·mL^{-1}, (d) 4 mg·mL^{-1}

Fig.6 Effect of amount of Mn-MOF derivative micromotors (left) and effect of time (right) on degradation of MB

Mn_2O_3 micromotors, the absorbance of MB was getting lower and lower. It indicates that the degradation efficiency is positively correlated with the amount of Mn_2O_3 micromotors. As shown in the right panel of Fig. 6, the absorption peak of MB gradually decreased with time going, which proves that the Mn_2O_3 micromotor has high degradation efficiency compared to static adsorption.

Harnessing excellent autonomous motion and catalytic performance of MOF derivative micromotors, they hold great potential for environmental applications. Table 1 lists some specific applications of the same type of Mn_2O_3 micromotors in environmental remediation. Compared with them, these Mn_2O_3 micromotors have the facile design strategy, lower material and production costs, as well as higher degradation efficiency for organic pollutants.

Table 1　Micro/nanomotors based on MOF derivatives in the field of environmental remediation

Type of micromotor	Morphology	Fabrication	Application	Time of removal / min	Ref.
Fe-zeolite	Janus particles	Solid-state ion exchange and ion sputtering processes	Degradation of phenol	90	[24]
Eu-MOF/EDTA-NiAl-CLDH/MnO_2	Microtubes	Chemical coprecipitation	Removal of Fe^{3+}	120	[38]
Ag-ZIF	Janus particles	Solvothermal	Degradation of RhB	150	[39]
Fe_2O_3	Octahedra	Decomposition	Adsorption of MB	5	[16]
Mn_2O_3	Spheroidal	Decomposition	Degradation of MB	5	This work

3　Conclusions

In conclusion, Mn-MOF derivative (Mn_2O_3) micromotors were successfully synthesized by thermal decomposition of Mn-MOF. The Mn-MOF derivatives present perfect spherical morphology with rough surface and pore characteristics. In addition, Mn_2O_3 micromotors show excellent catalytic activity and efficient autonomous mobility in H_2O_2. With the increase of H_2O_2 concentration, the speed of Mn_2O_3 micromotors was increased. It can reach 81.3 $\mu m \cdot s^{-1}$ in 10% H_2O_2 with an average lifetime of about 30 min. At the same time, Mn_2O_3 micromotors exhibit a Fenton-like effect in H_2O_2, which can efficiently degrade MB in water.

Supporting information is available at http://www.wjhxxb.cn

References:

[1]Guix M, Weiz S M, Schmidt O G, Medina-Sánchez M. Self-Propelled Micro/Nanoparticle Motors. *Part. Part. Syst. Charact.*, **2018**, **35**(2): 1700382

[2]Wang Q L, Dong R F, Yang Q X, Wang J J, Xu S Y, Cai Y P. Highly Efficient Visible-Light-Driven Oxygen-Vacancy-Based $Cu_{2+1}O$ Micromotors with Biocompatible Fuels. *Nanoscale Horiz.*, **2020**, **5**(2): 325-330

[3]Cai L J, Wang H, Yu Y R, Bian F K, Wang Y, Shi K Q, Ye F F, Zhao Y J. Stomatocyte Structural Color Barcode Micromotors for Multiplex Assays. *Natl. Sci. Rev.*, **2020**,**7**(3):644-651

[4]Wang D L, Gao C Y, Wang W, Sun M M, Guo B, Xie H, He Q. Shape-Transformable, Fusible Rodlike Swimming Liquid Metal Nanomachine. *ACS Nano*, **2018**,**12**(10):10212-10220

[5]Yoshizumi Y, Honegger T, Berton K, Suzuki H, Peyrade D. Trajectory Control of Self-Propelled Micromotors Using AC Electrokinetics. *Small*, **2015**,**11**(42):5630-5635

[6]Wang H, Liang Y L, Gao W, Dong R F, Wang C Y. Emulsion Hydrogel Soft Motor Actuated by Thermal Stimulation. *ACS Appl. Mater. Interfaces*, **2017**,**9**(49):43211-43219

[7]Liu W J, Ge H B, Ding X Y, Lu X L, Zhang Y N, Gu Z W. Cubic Nano-Silver-Decorated Manganese Dioxide Micromotors: Enhanced Propulsion and Antibacterial Performance. *Nanoscale*, **2020**, **12**(38): 19655-19664

[8]Schattling P S, Ramos-Docampo M A, Salgueiriño V, Städler B. Double-Fueled Janus Swimmers with Magnetotactic Behavior. *ACS Nano*, **2017**,**11**(4):3973-3983

[9]Maria-Hormigos R, Jurado-Sánchez B, Escarpa A. Surfactant-Free β-Galactosidase Micromotors for "On-The-Move" Lactose Hydrolysis. *Adv. Funct. Mater.*, **2018**,**28**(25):1704256

[10]Ma X, Hortelao A C, Miguel-López A, Sánchez S. Bubble-Free Propulsion of Ultrasmall Tubular Nanojets Powered by Biocatalytic Reactions. *J. Am. Chem. Soc.*, **2016**,**138**(42):13782-13785

[11]Ma X, Jang S, Popescu M N, Uspal W E, Miguel-Lopez A, Hahn K, Kim D P, Sánchez S. Reversed Janus Micro/Nanomotors with Internal Chemical Engine. *ACS Nano*, **2016**,**10**(9):8751-8759

[12]Moo J G S, Wang H, Pumera M. Influence of pH on the Motion of Catalytic Janus Particles and Tubular Bubble-Propelled Micromotors. *Chem. Eur. J.*, **2016**,**22**(1):355-360

[13]Wei X L, Beltrán-Gastélum M, Karshalev E, de Ávila B E F, Zhou J R, Ran D N, Angsantikul P, Fang R H, Wang J, Zhang L F. Biomimetic Micromotor Enables Active Delivery of Antigens for Oral Vaccination. *Nano Lett.*, **2019**,**19**(3):1914-1921

[14]Zhou M F, Hou T, Li J X, Yu S S, Xu Z J, Yin M, Wang J, Wang X L. Self-Propelled and Targeted Drug Delivery of Poly(aspartic acid)/Iron-Zinc Microrocket in the Stomach. *ACS Nano*, **2019**,**13**(2):1324-1332

[15]Chen B R, Sun W H, Kitchaev D A, Mangum J S, Thampy V, Garten L M, Ginley D S, Gorman B P, Stone K H, Ceder G, Toney M F, Schelhas L T. Understanding Crystallization Pathways Leading to Manganese Oxide Polymorph Formation. *Nat. Commun.*, **2018**, **9**: 2553

[16]Peng X, Zhu H L, Chen H J, Feng X M, Liu R Q, Huang Z D, Shen Q M, Ma Y W, Wang L H. Eco-Friendly Porous Iron(Ⅲ) Oxide Micromotors for Efficient Wastewater Cleaning. *New J. Chem.*, **2019**, **43** (32):12594-12600

[17]Keller S, Teora S P, Hu G X, Nijemeisland M, Wilson D A. High-Throughput Design of Biocompatible Enzyme-Based Hydrogel Microparticles with Autonomous Movement. *Angew. Chem. Int. Ed.*, **2018**,**57**(31):9814-9817

[18]Novotný F, Plutnar J, Pumera M. Plasmonic Self-Propelled Nanomotors for Explosives Detection via Solution-Based Surface Enhanced Raman Scattering. *Adv. Funct. Mater.*, **2019**,**29**(33):1903041

[19]Wang D L, Gao C Y, Zhou C, Lin Z H, He Q. Leukocyte Membrane-Coated Liquid Metal Nanoswimmers for Actively Targeted Delivery and Synergistic Chemophotothermal Therapy. *Research*, **2020**:UNSP 3676954

[20]Jurado-Sánchez B, Wang J. Micromotors for Environmental Applications: A Review. *Environ. Sci.-Nano*, **2018**,**5**(7):1530-1544

[21]Li J X, Gao W, Dong R F, Pei A, Sattayasamitsathit S, Wang J. Nanomotor Lithography. *Nat. Commun.*, **2014**,**5**:5026

[22]Neoh C H, Noor Z Z, Mutamim N S A, Lim C K. Green Technology in Wastewater Treatment Technologies: Integration of Membrane Bioreactor with Various Wastewater Treatment Systems. *Chem. Eng. J.*, **2016**,**283**:582-594

[23]Liang C Y, Zhan C, Zeng F Y, Xu D D, Wang Y, Zhao W W, Zhang J H, Guo J H, Feng H H, Ma X. Bilayer Tubular Micromotors for Simultaneous Environmental Monitoring and Remediation. *ACS Appl. Mater. Interfaces*, **2018**,**10**(41):35099-35107

[24]Ma W, Wang K, Pan S H, Wang H. Iron-Exchanged Zeolite Micromotors for Enhanced Degradation of Organic Pollutants. *Langmuir*, **2020**,**36**(25):6924-6929

[25]Shi H Q, Chen X, Liu K, Ding X Y, Liu W J, Xu M L. Heterogeneous Fenton Ferroferric Oxide-Reduced Graphene Oxide-Based Composite Microjets for Efficient Organic Dye Degradation. *J. Colloid Interface Sci.*, **2020**,**572**:39-47

[26]Mou F Z, Pan D, Chen C R, Gao Y R, Xu L L, Guan J G. Magnetically Modulated Pot-like $MnFe_2O_4$ Micromotors: Nanoparticle Assembly Fabrication and Their Capability for Direct Oil Removal. *Adv. Funct. Mater.*, **2015**,**25**(39):6173-6181

[27]Baptista-Pires L, Orozco J, Guardia P, Merkoçi A. Architecting Graphene Oxide Rolled-Up Micromotors: A Simple Paper-Based Manufacturing Technology. *Small*, **2018**,**14**(3):1702746

[28]Villa K, Parmar J, Vilela D, Sanchez S. Metal-Oxide-Based Microjets for the Simultaneous Removal of Organic Pollutants and Heavy Metals. *ACS Appl. Mater. Interfaces*, **2018**,**10**(24):20478-20486

[29]Hou T, Yu S, Zhou M F, Wu M, Liu J, Zheng X L, Li J X, Wang J, Wang X L. Effective Removal of Inorganic and Organic Heavy Metal Pollutants with Poly(amino acid)-Based Micromotors. *Nanoscale*, **2020**,**12**(8):5227-5232

[30]Khezri B, Pumera M. Metal-Organic Frameworks Based Nano/Micro/Millimeter-Sized Self-Propelled Autonomous Machines. *Adv. Mater.*, **2019**,**31**(14):e1806530

[31]Ikezoe Y, Washino G, Uemura T, Kitagawa S, Matsui H. Autonomous Motors of a Metal-Organic Framework Powered by Reorganization of Self-Assembled Peptides at Interfaces. *Nat. Mater.*, **2012**,**11**: 1081-1085

[32]Chen H J, Zhu H L, Huang J, Feng X M. Shape-Controlled Catalytic ZIF-67 Micromotors for Dye Adsorption. *J. Mater. Eng. Perform.*, **2020**,**29**:6196-6200

[33]Zhang H J, Qi S D, Niu X Y, Hu J, Ren C L, Chen H L, Chen X G. Metallic Nanoparticles Immobilized in Magnetic Metal-Organic Frameworks: Preparation and Application as Highly Active, Magnetically Isolable and Reusable Catalysts. *Catal. Sci. Technol.*, **2014**, **4** (9):3013-3024

[34]Zou G Q, Hou H S, Cao X Y, Ge P, Zhao G G, Yin D L, Ji X B. 3D Hollow Porous Carbon Microspheres Derived from Mn-MOFs and Their Electrochemical Behavior for Sodium Storage. *J. Mater. Chem. A*, **2017**,**5**(45):23550-23558

[35]Zhang X D, Lv X T, Bi F K, Lu G, Wang Y X. Highly Efficient Mn_2O_3 Catalysts Derived from Mn-MOFs for Toluene Oxidation: The Influence of MOFs Precursors. *Mol. Catal.*, **2020**,**482**:110701

[36]Cao H Q, Wu X M, Wang G H, Yin J F, Yin G, Zhang F, Liu J K. Biomineralization Strategy to α-Mn_2O_3 Hierarchical Nanostructures. *J. Phys. Chem. C*, **2012**,**116**(39):21109-21115

[37]Yao Y Y, Cai Y M, Lu F, Wei F Y, Wang X Y, Wang S B. Magnetic Recoverable $MnFe_2O_4$ and $MnFe_2O_4$-Graphene Hybrid as Heterogeneous Catalysts of Peroxymonosulfate Activation for Efficient Degradation of Aqueous Organic Pollutants. *J. Hazard. Mater.*, **2014**,**270**: 61-70

[38]Yang W N, Li J, Xu Z P, Yang J, Liu Y, Liu L H. An Eu-MOF/EDTA-NiAl-CLDH Fluorescent Micromotor for Sensing and Removal of Fe^{3+} From Water. *J. Mater. Chem. C*, **2019**,**7**(33):10297-10308

[39]Wang R Q, Guo W L, Li X H, Liu Z H, Liu H and Ding S Y. Highly Efficient MOF-Based Self-Propelled Micromotors for Water Purification. *RSC Adv.*, **2017**,**7**(67):42462-42467